On Large Structures and Turbulent Mixing in Confined Mixing Layers under Forcing

G. R. Wang
Hermann-Föttinger-Institut für Strömungsmechanik, Technische Universität, Berlin, Germany

DOI 10.1002/aic.10615
Published online September 12, 2005 in Wiley InterScience (www.interscience.wiley.com).

New phenomena have been observed experimentally in a novel rapid mixing process, where a confined mixing layer in a pipe is periodically forced, especially under strong forcing. In the confined configuration without forcing, there are two incommensurable peaks in the scalar power spectrum: one corresponds to the well-known Kelvin–Helmholtz instability, but the other is not known, having a narrow-frequency band around a nearly constant frequency that is independent of the mean flow velocity. With strong forcing within the narrow-frequency band, the spreading angle of the mixing layer is not restrained by the well-known saturation phenomenon, but could even achieve a quasi-180 ° immediately downstream of the trailing edge, exhibiting an extraordinarily fast mixing. The mixing layer not only biases to the low-speed side as the conventional mixing layer does, it could also be symmetric to the splitterplate and even bias to the high-speed side. These phenomena can be observed only when the forcing is within the narrow-frequency band. We also find that the streamwise vortices, which result from interaction between the primary vorticity and the vorticity originating from the streamwise corner flow between the splitterplate and sidewall immediately downstream of the trailing edge of the splitterplate, could play an important role for these new observations. These streamwise vortices are very sensitive to initial periodic forcing at the narrow-frequency band and amplify very fast. The results indicate that the confined mixing layer in a pipe is a very interesting flow.
 AIChE J, 52: 111–124, 2006
Keywords: mixing, turbulence, transport, fluid mechanics, mass transfer

Introduction

Fluid mixing is of surpassing interest in science and engineering applications.[1-4] In many cases, we need fast mixing, such as in combustion,[5] acoustic noise reduction,[6] and protein folding in biotechnology.[7] Traditionally, agitated tank and static mixer,[8,9] jet, and mixing layer[10,11] are often used to enhance mixing. Other mixing augmentation methods include chaotic mixing at relatively low Reynolds number flows[12,13] and an oscillatory flow mixer consisting of tubes fitted with equally spaced orifice plate baffles.[14]

Recently, Wang[15,16] introduced a novel extremely fast mixing process in a confined three-dimensional mixing layer in a pipe (that is, the inlet of the pipe is a mixing layer), where the initial two streams can be mixed, at least on the large scale, within one pipe diameter downstream of the splitterplate. The rapid mixing can also be obtained at relatively small Reynolds number flow in this confined configuration, where the Reynolds number is 400 based on the mean velocity and pipe diameter and the original flow is laminar without forcing. For this relatively small Reynolds number flow, the scalar power spectrum can display $-5/3$ Obouk-hov–Corrsin spectrum in the near field under strong forcing. This could have a substantial impact in technologies that require fast mixing, both in laminar and turbulent flows. Such an interesting flow could also be a new candidate for homogeneous turbulence

The present address of G. R. Wang: CFD Research Corporation, 215 Wynn Dr., Huntsville, AL 35805.
Correspondence concerning this article should be addressed to G. R. Wang at guirenwang@yahoo.com.

study in relatively low Reynolds number flow. The work is based on the receptivity and control of large coherent structures in turbulent flows.

Brown and Roshko[17] discovered that in the mixing layer, the large spanwise coherent structures played an important role for mixing, that is, the entrainment and spreading rate of the mixing layer. Winant and Browand[18] demonstrated that successive vortex mergings were the primary processes governing the streamwise spreading of the mixing layer. The development of these large structures can be described by Kelvin–Helmholtz instability (see, for example, Michalke,[19,20] Bechert,[21] and Huerre and Monkewitz[22]). The unstable wave of the primary vortex is determined by the initial most-probable frequency and is very sensitive to initial external disturbance, and can therefore be controlled with initial external disturbance.[23] Thus, forcing the mixing layer to enhance mixing was the focus of investigations by Oster et al.,[24] Oster and Wygnanski,[25] Ho and Huang,[26] Fiedler and Mensing,[27] Nygaard and Glezer,[28] Wiltse and Glezer,[29] and many others. An important common conclusion from these works is that the spreading rate, which is one of the most important fundamental parameters and is often used as a mixing criterion in the mixing layer (see, for example, Cantwell[30] and Dimotakis[31]), can be enhanced through the active forcing.

Unfortunately the effect of conventional initial periodic forcing in mixing layers for mixing enhancement is limited by the saturation phenomenon arising from the nonlinear effect.[24,25] For instance, Fiedler and Mensing[27] observed the saturation when the forcing amplitude was sufficiently high, that is, the intensity of the maximum periodic transverse velocity constituents and saturation Strouhal number became constant and independent of forcing amplitude when the forcing amplitude was $>6.5\%$. They obtained the same mean spreading rate for both strong and weak forcing, that is, twice the neutral value and independent of forcing amplitude. Weisbrot and Wygnanski[32] also investigated strong forcing and reported no distinguishing difference in the spreading rate from that of Fiedler et al.[33] and Oster and Wygnanski.[25] On the foundation of the above-mentioned observations and that of others, Browand and Ho[34] proposed a quasi-universal spreading rate of the forced and unforced mixing layers.

In the confined mixing layer, however, Wang[15,16] surprisingly found that the aforementioned saturation limitation of the spreading rate of the shear layer could be overcome when the flow was forced under a specific narrow-frequency band. Thus, the mixing can be dramatically enhanced with increasing the forcing amplitude. The author designed such a confined mixing layer in a pipe initially in an effort to experimentally verify his phenomenological model on "ideal turbulent mixing process and state" to investigate fundamental turbulent mixing. The confined configuration was designed to reduce mixing time of the initial two streams to achieve fast mixing. The circular pipe was chosen to avoid the complexity of the corner flow distortion of the large coherent structures in the conventional mixing layer in a channel of rectangular cross section because the corner flows could become more effective in the confined configuration.

However, no details of the vortex dynamics of the confined mixing layer, corresponding to the external periodic forcing, were presented in Wang,[16] and the physical mechanism of the interesting flow and fast mixing process is still not clear. The motivation for this investigation reported herein is to introduce these phenomena to stimulate further study of the mechanism. We shall concentrate on the spreading rate of the mixing layer, streamwise vortices, and their responses to the forcing. We shall show that, on the one hand, many basic phenomena in the conventional two-dimensional mixing layer can also be observed in the three-dimensional mixing layer despite the complex sidewall effect; on the other hand, the sidewall effect not only adds extra complex and quantitative variations, but also causes interesting phenomena under strong forcing, which to the author's knowledge, have never been reported.

Experimental Setup

The experimental configuration is shown in Figure 1. The details are reported in Wang.[15] Two vessels of 300 L at 2.5 m higher than the test section supplied water and aqueous solution (laser dye) to a water channel. The water level changed little during the 30-s run so that the fluid velocity was almost constant. One vessel was filled with water and the other with aqueous fluorescein disodium solution. Rotameters were used to control and measure the mean flow velocity in the test section. The two streams flowed into a settling chamber through the sidewall, respectively. The settling chamber upstream of a nozzle was 400 mm long, and had one honeycomb and two screens. The nozzle that was designed in light of Börger's theory[35] had a contraction ratio of 10:1 and was 100 mm long. In the axial symmetrical center of settling chamber and nozzle there was a splitterplate, which had a uniform thickness of 5 mm in the settling chamber and a sharp trailing edge at the end of the nozzle. The water stream and dye solution stream flowed on the top and bottom of the splitterplate, respectively. A polypropylene pipe (42 mm ID; 4 mm thick; 2.1 m total length) was connected with the nozzle as the test section. At the downstream position from the trailing edge, $x = 1$ m, there was a cube of 100 mm length, in the middle of which a mirror M4 of 40 $\times$ 40 mm was placed for visualization. The mirror surface was disposed with 45 ° to the pipe axis. The cross section of the cube was large enough so that the blockage of the mirror had no influence on the near field flow in the test section.

The mixing layer was forced by two different methods. The first one involved a loudspeaker as the actuator, which was located near the input of the settling chamber in the axial direction on the low-speed side. The speaker excited the flow through the connection of a rubber membrane, which in turn was connected directly to the water stream. Because of the water's high pressure, the membrane was under substantial tension, such that it could not be forced to move by the speaker. For this reason, a sealed bottle was used in connection with the speaker, the latter also being sealed. The bottle, half-filled with water, was connected with the fluid in the settling chamber through a tube. The air in the bottle was connected with the speaker. If the pressure in the settling chamber was increased, the pressure in the bottle would also rise, which resulted in a pressure increment on the speaker side of the membrane, so that the membrane could avoid the tension and be able to vibrate. A condenser was constructed between the speaker and membrane to measure the amplitude of the membrane displacement. The condenser was connected to a frequency bridge, which was connected to an oscilloscope. To read the displace-

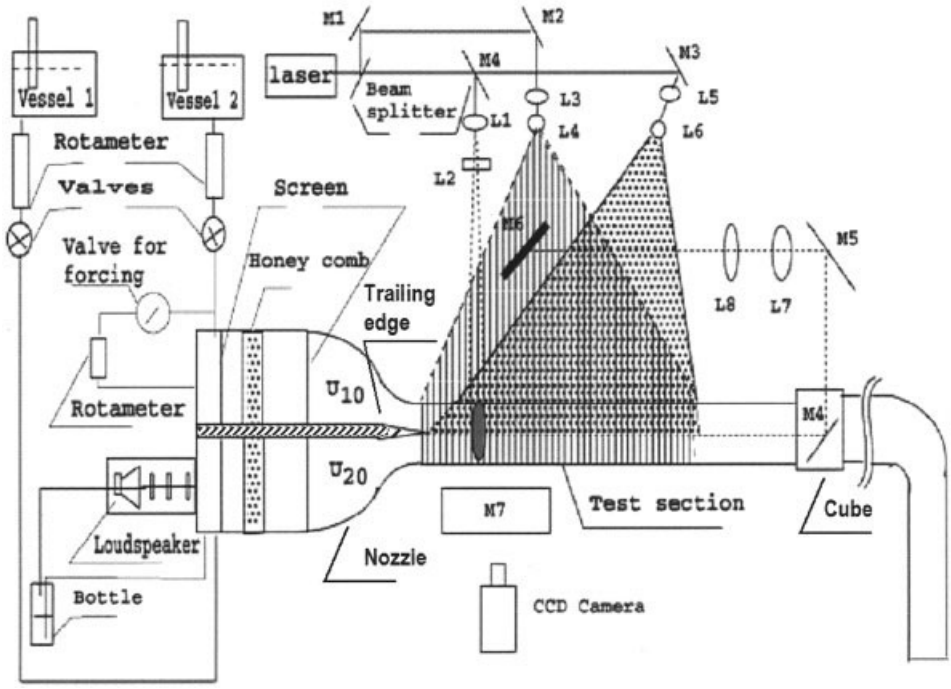

Figure 1. Experimental.

L = lens; M = mirror.

ment, a stroboscope was used. A linear relationship between the amplitude of the speaker and the signal from the frequency bridge had been calibrated before use. Through this construction the forcing amplitude of the speaker can be measured. An HP 33120A signal generator supplied sinusoid signals that were amplified with a DFVLR power amplifier for the speaker. The forcing was actually monitored with an oscilloscope and shown as sinusoidal. Because the speaker could not provide sufficient power for flows of higher Reynolds number, a rotating valve was used for the forcing as an alternative. The high-speed fluid was first divided into two streams. One stream passed a valve for forcing, which could be driven to rotate by a motor. The rotation of the valve for forcing resulted in a periodic blocking of the flow, and thus a periodic velocity. The forcing frequency was controlled through the speed of the motor and forcing amplitude through the ratio of flow rates of the two streams. No apparent difference of the mixing layer evolution could be observed between the two forcing methods.

Laser-induced fluorescence (LIF) was applied here for the flow visualization with a 5-W Coherent Inova 90 argon laser. Fluorescein disodium was used as the dye. The peaks of absorption and emission spectrum of the fluorescein are blue (488 nm) and green (530 nm), respectively. Because the reflecting laser light from the pipe was strong, the excitation light of the laser should be different from the emitting one in the wavelength, to get clear pictures with minimum reflecting light. Using an etalon we could get only blue color (488 nm) light. To filter away the reflecting light, a narrow optical band filter (500–600 nm) and a yellow color filter were, in series, placed in front of a Sony CCD camera, which was used to record the images. Cylinder lenses were used to achieve two-dimensional light sheets to visualize side, plane, and cross-views of the mixing layer. The optical system is also shown in Figure 1.

The most-probable frequency, close to the theoretical most-amplified frequency,[26] was measured through the dye scalar point measurement with the LIF in the mixing layer.[36] Because the measuring point was before the first rollup of the primary vortex, the frequency corresponding to the peak in the power spectrum should approximately represent the initial unstable wave frequency. An HP 3562A Dynamic Signal Analyzer was used to record the power spectrum.

The initial momentum thickness, often used for the scaling in the mixing layer,[23] could be approximately estimated through two-dimensional spatial mode of linear instability theory, given that the flow was approximately two-dimensional immediately downstream of the trailing edge without forcing. Without forcing, the Strouhal number $\mathrm{St}_0 = \theta_0 f_{01}/\bar{U}$ corresponding to the most-amplified frequency f_{01} of Kelvin–Helmholtz instability is a constant (that is, nearly 0.032), where θ_0 denotes the sum of the initial momentum thickness θ of the mixing layer without forcing; $\bar{U} = (U_1 + U_2)/2$ represents the mean flow velocity; and U_1 and U_2 are the initial mean flow velocity of the two streams, respectively. Therefore, with the measured f_{01} and $\bar{U}$, θ_0 could be calculated. The estimated initial Reynolds number based on initial momentum thickness is $\mathrm{Re}_{\theta_0} = \theta_0 \bar{U}/\nu$.

The visualized scalar structure sizes, their corresponding mixing layer thickness δ_ν, and spreading rated $\delta\nu/dx$ were used as the criteria of mixing,[30] even though the instability theory and receptivity are usually described by the disturbance of velocity. The reason is that, in the beginning of the mixing layer, the higher the coherent composition of the velocity, the larger its corresponding vortex, which can be recognized by the large scalar structures. The receptivity here means the external forcing energy is converted into the unstable wave of velocity.

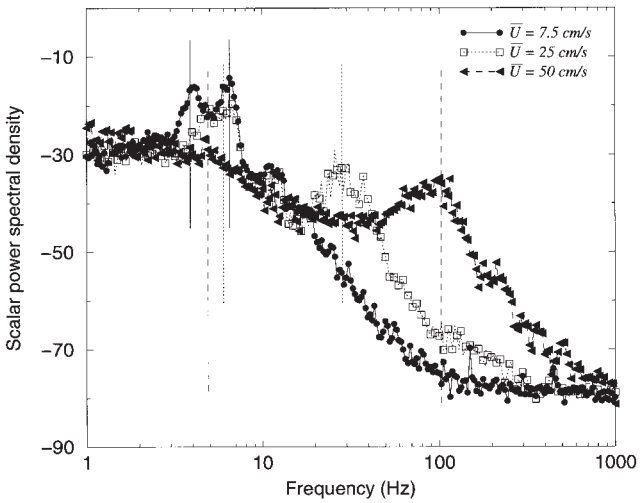

Figure 2. Scalar power spectrum in unforced mixing layers for various $\bar{U}$ values at a constant $\lambda = 0.2$.

Each $\bar{U}$ has two peaks in its power spectrum, which was obtained through point measurement of an extremely high spatial resolution of about $(4\ \mu m)^3$ with LIF in the middle of the mixing layer at $x/D = 0.7$. The vertical lines mark the locations of the two peaks of the power spectra for each curve. The solid lines, dotted lines, and dashed lines are for the cases of $\bar{U} = 7.5$, 25, and 50 cm/s, respectively.

The relative average forcing amplitude resulting from the membrane was approximately described as

$$A_f = \sqrt{\tilde{u}_f^2}/\bar{U}(\%) = 2a_M f_f (A_M/A_N)/(1.414\bar{U}) \qquad (1)$$

where the ratio of membrane to nozzle area A_M/A_N was 2 in the setup. $\tilde{u}_f$ is the disturbance of streamwise velocity component, f_f denotes forcing frequency, and a_M represents the maximum displacement of the membrane. A_f represents only the external forcing amplitude and could be different from the real coherent velocity component at the trailing edge. Their relation is unknown and could depend on the transfer function between the A_f and the real coherent velocity component at the trailing edge or the receptivity at the trailing edge of the setup.

Results

The visualization was undertaken in the near field of the mixing layers. The fluids flowed from left to right for the side views. The laser sheet for the side views propagated from top to bottom through the axis of the pipe. The trailing edge of the splitterplate was within the view of the pictures on the left side.

Most-probable frequency

For a conventional mixing layer, the Strouhal number St_0, corresponding to the most probable frequency f_{01} of the Kelvin–Helmholtz instability, is a constant and f_{01} scales with $\bar{U}^{3/2}$.[23] Figure 2 shows the scalar power spectrum $E(f)$ for the unforced mixing layer with three different mean flow velocities at $x/D = 0.7$, where x is the streamwise position from the trailing edge and D denotes the inner diameter of the pipe. For the three cases in Figure 2, values of $\bar{U}$ were 7.5, 25, and 50 cm/s, respectively, with a constant velocity ratio $\lambda = (U_1 - U_2)/(U_1 + U_2) = 0.2$. It was found that for each given $\bar{U}$ in Figure 2, the scalar power spectrum had two peaks, one of which approximately increased with $\bar{U}^{3/2}$ and the other was approximately a constant around 6 Hz in a very narrow frequency band (the corresponding quasi–6 Hz of the primary structure can also be seen in Figure 10 for the case of $\bar{U} = 25$ cm/s). We call the nearly constant frequency corresponding to the new peak as f_{02}. The two frequencies corresponding to the peaks were not commensurate, that is, the low frequency was not the subharmonic of the higher one.

Relations between the frequency corresponding to the peaks in the power spectrum and $\bar{U}$ are displayed in Figure 3, demonstrating again that one approximately increased with $\bar{U}^{3/2}$, but the other was approximately a constant within a narrow-frequency band between 5 and 7 Hz. Obviously the one that scaled with $\bar{U}^{3/2}$ corresponded to the conventional most-probable frequency f_{01} of the Kelvin–Helmholtz instability in the two-dimensional mixing layer; the other was f_{02}. However, it is not clear why there is a peak near 6 Hz for all the flows. Because Ho and Huang[26] suggested that f_{01} scaled with the boundary layer thickness of the high-speed side of the trailing edge, λ used for Figure 3 was a constant of 0.33 to avoid the θ_0 effect. Figure 3 was actually not limited to $\lambda = 0.33$; it was also applicable to other values of λ and $\bar{U}$. The $\bar{U}$ used was in the range of 1–80 cm/s and λ in 0–1. f_{02} was almost a constant and independent of $\bar{U}$ and λ within this range. The highest possible values of U_1 and U_2 that could be provided in the present experimental apparatus were 120 and 40 cm/s, respectively. Its corresponding f_{02} was also about 6 Hz.

Figures 2 and 3 demonstrated that the behavior of the most-probable frequency observed in a conventional two-dimensional mixing layer could also be observed in the highly three-dimensional mixing layer. However, there was also an extra unknown constant frequency in the current confined configuration—this is not a trivial finding! In the following, we will see that it is just under the forcing of this quasi-constant frequency that the flows show interesting phenomena, such as mixing enhancement.

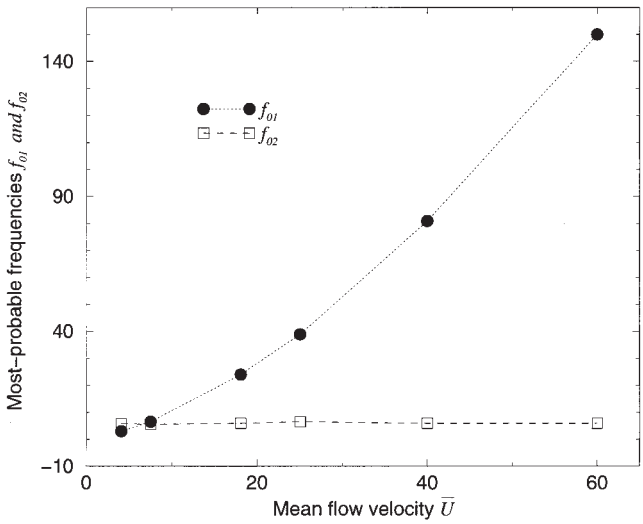

Figure 3. Relationship of f_{01}, f_{02} with $\bar{U}$ for a constant $\lambda = 0.33$.

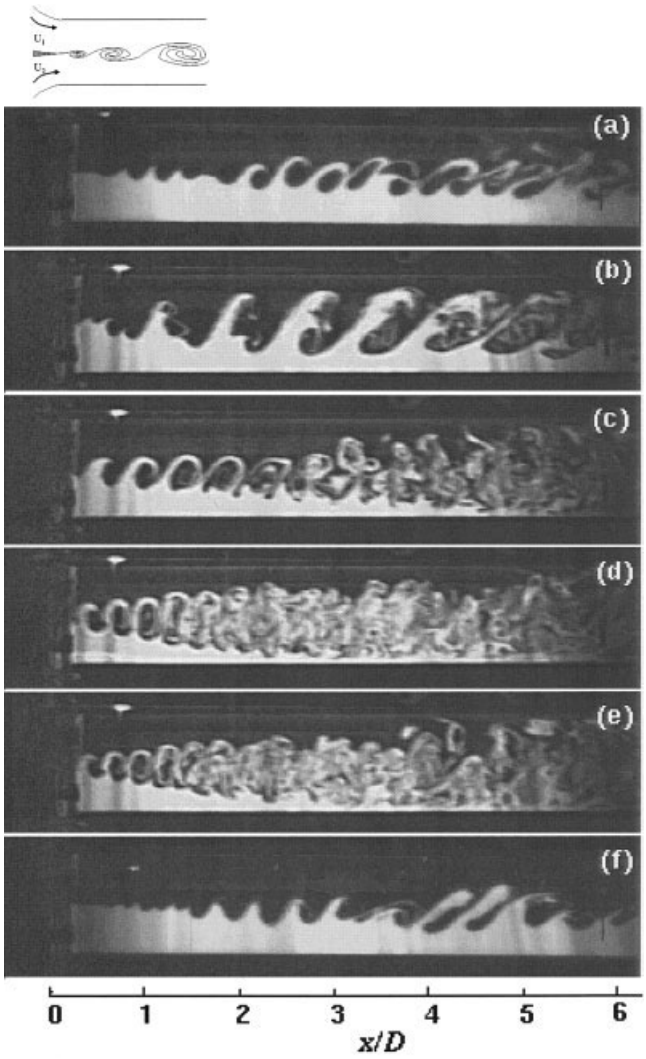

Figure 4. Influence of f_f for the mixing layer with U_1 = 9 cm/s and U_2 = 6 cm/s under a constant A_f of about 7%.

(a) f_f = 0 Hz (unforced case); (b) 2.4 Hz; (c) 4.4 Hz; (d) 6.0 Hz; (e) 7.2 Hz; (f) 9.0 Hz.

Forcing frequency effect

Figure 4 (side view) illustrates the influence of forcing frequency f_f with a constant forcing amplitude A_f. The trailing edge position is also shown in Figure 4 and is the same for all other side view images shown herein. The initial speeds of the two streams were U_1 = 9 cm/s and U_2 = 6 cm/s, respectively; f_f changed in the range of 2.4–9 Hz and A_f was about 7%, that is, strong forcing. Figure 4a was the case without forcing. The f_{01} value of Kelvin–Helmholtz vortices was estimated to be 7.2 Hz, a value that was slightly higher than its corresponding value in Figure 2, given that $E(f)$ was measured at $x/D > 0$, and the measured frequencies decreased with increasing x. Note that with the increasing value of $\bar{U}$, the relative difference between the measured frequency at the measuring point and the vortex passage frequency at the beginning of the mixing layer decreases. No apparent difference could be observed between the confined mixing layer and conventional two-dimensional mixing layer according to Figure 4a. Figure 4b denotes the case of f_f = 2.4 Hz. Because this was in the second subharmonic region, that is, in mode III according to Ho and Huang,[26] the tripling of vortices was observed in the initial stage. The shear layer spread fast as the three vortices were merging. After the merging, the shear layer was in the frequency-lock region and did not spread until x/D = 4.8. In Figure 4c the mixing layer was forced at f_f = 4.4 Hz. Because this was between the f_{01} and its first subharmonic, that is, in mode I, no vortex merging was found in the initial stage. The frequency-lock region approximately followed the first rollup. Compared with the unforced one, $d\delta_v/dx$ was increased immediately downstream of the trailing edge with forcing.

Figure 4d was also in the mode I as the case of Figure 4c, but with higher f_f = 6 Hz and closer to f_{01}. According to Ho and Huang,[26] the development of the mixing layer in Figure 4d should be similar to that in Figure 4c, except that the primary vortex size in Figure 4d should be smaller than that in Figure 4c. Surprisingly, however, there was no frequency-lock region in Figure 4d, and the mixing layer spread more or less linearly until the edge of the low-speed side of the mixing layer reached the wall. During this spreading process, no subharmonic component could be observed. The average $d\delta_v/dx$ was higher than that of Figure 4c. Figure 4e was forced at 7.2 Hz. The mixing layer evolution in Figure 4e was similar to that of Figure 4d. However, the vortex size in transverse direction and its corresponding $d\delta_v/dx$ in Figure 4e were smaller than those in Figure 4d, but larger than those in Figure 4c in the near field. In Figure 4f where f_f was 9 Hz, there was, as expected, a slight decrease of $d\delta_v/dx$ compared with the unforced one in the initial stage. The results from Figures 4a, 4b, 4c, and 4f were similar to those from Ho and Huang[26] and Oster and Wygnanski[25] in the conventional two-dimensional mixing layer.

The point of interest is the comparison among Figures 4c, 4d, and 4e. As we know from Ho and Huang[26] that in mode I, the vortical sizes following the trailing edge decrease with the increase of forcing frequency. For this reason, the vortices in Figure 4e should be smaller than those in Figure 4d, which in turn, should be smaller than those in Figure 4c. However, the vortical size in Figure 4d was larger than that in Figure 4c in the transverse direction after x/θ_0 = 63 (x/D = 0.5). The frequency-lock region in Figure 4c disappeared in Figure 4d. With further increase of f_f, as shown in Figures 4e and 4f, the vortical sizes again became smaller compared with that in Figure 4d. Many experiments showed that, barring the possibility of an experimental error, the forcing at 6 Hz had a higher value of $d\delta_v/dx$ than that at other values of f_f. Therefore f_f = 6 Hz had the maximum $d\delta_v/dx$. Note that usually the vortex merging biased to the low-speed side of the mixing layer.[33] However, the merging in Figure 4b seemed to bias to the high-speed side, which could be related to a phenomenon called "pairing burst." [15,37]

Figure 4 also shows that the confined mixing layer has a similar response to the forcing, compared to a two-dimensional mixing layer. However, the difference was also observed when the flow was forced near 6 Hz. Note that the $d\delta_v/dx$ at f_f = 7.2 Hz in Figure 4e was higher than that at 4.4 Hz in Figure 4c and the development of the mixing layer in Figure 4d was similar to that in Figure 4e. This could indicate that at f_f = 7.2 Hz, the flow was influenced by both the Kelvin–Helmholtz instability and the unknown mechanism around f_f = 6 Hz.

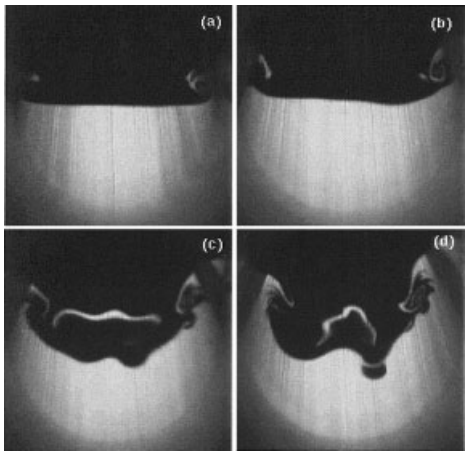

Figure 5. Evolution of the streamwise Type A vortices along streamwise positions in the mixing layer without forcing.

$U_1 = 9$ cm/s, $U_2 = 6$ cm/s. (a) $x/D = 0.2$; (b) 1; (c) 2; (d) 4.

Streamwise vortices

To understand the flow in the confined configuration, it is necessary to investigate its streamwise vortices. The cited new phenomenon of forcing around 6 Hz and other new phenomena to be discussed later in this work are closely related to the streamwise vortices. Note that in some cross-view pictures, there were two sharp dark areas (see, for instance, Figure 9g below), where the laser sheet propagated from top to bottom, explained by the fact that the pipe wall could act as a lens and form these dark areas.

Evolution of the streamwise vortices in the unforced mixing layers, is shown in Figure 5 with $U_1 = 9$ cm/s and $U_2 = 6$ cm/s. Interaction between the vorticity, which originated from the four corner flows between the splitterplate and sidewall, and the spanwise vorticity in the mixing layer resulted in counter-rotating vortex pairs, as shown in Figures 5a and 5b, where x/D was 0.2 and 1, respectively (these vortices were visible, but of poor quality because little dye is convected to the high-speed side in the initial stage). These streamwise vortices were at the high-speed side and were quasi-mirror symmetric to the vertical plane through the pipe axis. They were different from those streamwise vortices in conventional mixing layers and were the most important streamwise vortices in the confined configuration. We call them *Type A vortices* here.

Because the high-speed side had higher vorticity, these counterrotating vortex pairs were attracted into the high-speed side. During the evolution process downstream, the mixing layer biased to the low-speed side as a result of the momentum transfer from the high-speed fluid to the low-speed fluid. This would cause the high-speed fluid to move in the radially center region to the low-speed side and the low-speed fluid to the high-speed side symmetrically along the sidewall because of continuity. Thus, a secondary flow was created, which could be enhanced with increasing velocity ratio λ because the bias increased with λ. Without forcing, this motion also caused the Type A vortices to develop to the high-speed side along the sidewall as shown in Figures 5c and 5d, where x/D was 2 and 4, respectively, because the Type A vortices originated near the sidewall.

During the development of the mixing layer, the secondary flow and the vorticity of the low-speed side of Type A vortices strengthened each other. This could cause the Type A vortices in the low-speed side to become larger than those in the high-speed side as shown in Figure 5. Their size was the same only when λ was zero.[15] The difference depended on λ. The higher the value of λ, the greater the difference. The size of the Type A vortices was close to the size of primary vortices in the transverse direction.

In Figure 5a, except the Type A vortices, no spanwise wave could be found. The interface line between the high- and low-speed streams was straight. In Figure 5b, the straight line was distorted. The rollup process of primary vortex could be observed in Figure 5c, where the spanwise wavelength seemed to be close to the size of the Type A vortices. Here we could see the initially developed spanwise undulation, which could develop into streamwise vortex similar to that in two-dimensional mixing layers. The further development was shown in Figure 5d, where the spanwise undulation in Figure 5c became distorted by the primary vortices and the secondary flow.

The development of Type A vortices strongly depended on the forcing, such as f_f and A_f. When the flow was forced near 6 Hz, the evolution of Type A vortices was enhanced, as shown in Figure 6, where f_f was 5.6 Hz and A_f was about 6%. Compared with the unforced ones, the size of the Type A vortices of the high- and low-speed sides in the forced flow was almost the same, as shown in Figures 6a ($x/D = 0.2$) and 6b ($x/D = 1$). The Type A vortices became similar to those in a wake with $\lambda = 0$,[15] almost without the motion to the high-speed side. Further downstream at $x/D = 2$ and 4, the Type A vortices still developed very fast and almost reached the axis of the pipe in the spanwise direction, as shown in Figures 6c and 6d, respectively, where the aforementioned secondary flow was also enhanced. Here the amplification of the Type A vortices and the fluids mixing were largely enhanced under forcing compared with the unforced case in Figure 5.

Although the interface line between the high- and low-speed streams had no apparent undulation in the spanwise direction in

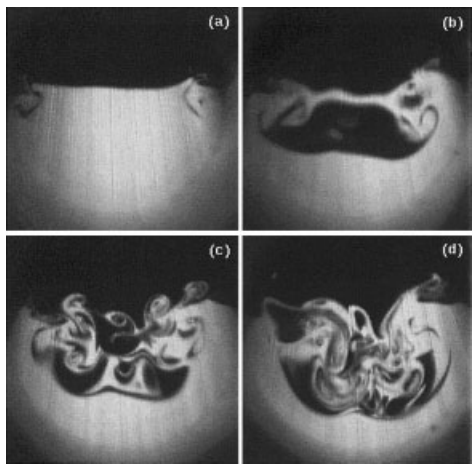

Figure 6. Evolution of the streamwise Type A vortices along streamwise positions in the mixing layer with forcing.

$U_1 = 9$ cm/s, $U_2 = 6$ cm/s, $f_f = 5.6$ Hz, A_f is around 6%. (a) $x/D = 0.2$; (b) 1; (c) 2; (d) 4.

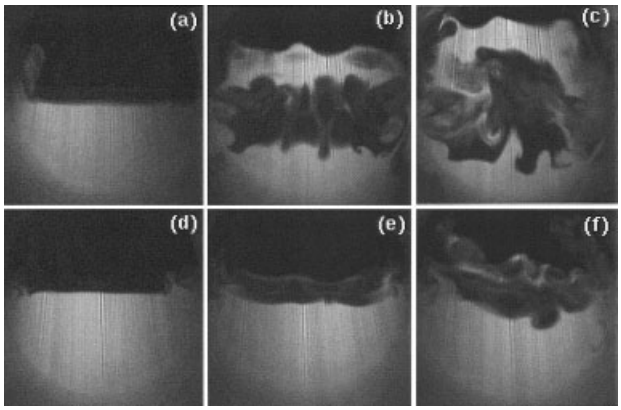

Figure 7. Comparison for the different responses of the streamwise vortices to the forcing at f_f = 6 and 16 Hz, respectively, with U_1 = 30 cm/s, U_2 = 20 cm/s, and A_f = 7%.

(a) f_f = 6 Hz, x/D = 0.2; (b) f_f = 6 Hz, x/D = 1; (c) f_f = 6 Hz, x/D = 2; (d) f_f = 16 Hz, x/D = 0.2; (e) f_f = 16 Hz, x/D = 1; (f) f_f = 16 Hz, x/D = 2.

Figure 6a, it was not as straight as the corresponding unforced one. In Figure 6b the undulation already became clear compared with the unforced one. With further evolution and interaction between the Type A vortices and primary vortices downstream, the undulation developed into the streamwise vortices, as displayed in Figures 6c and 6d. The positive impulse feedback between the Type A vortices and the aforementioned secondary flow was also enhanced in Figures 6c and 6d.

Figures 5 and 6 therefore indicate that the development of the originally two-dimensional mixing layer into the three-dimensional one is related to the Type A vortices and the secondary flow, and their interactions with the primary vortices. The forcing could enhance the evolution of the streamwise structures that, in turn, could accelerate the development from the originally two-dimensional mixing layer into the three-dimensional one in the confined configuration.

Another interesting phenomenon was that the Type A vortices amplified very fast only under strong forcing of the narrow-frequency band around f_f = 6 Hz. This is demonstrated in Figure 7, where U_1 = 30 cm/s and U_2 = 20cm/s. Figures 7a, 7b, and 7c are cross-views of Figure 10c at x/D = 0.2, 1, and 2, respectively, with f_f = 6 Hz. Figures 7d, 7e, and 7f (x/D = 0.2, 1, and 2, respectively) represent a forced case at f_f = 16 Hz (that is, in mode II) because f_{01} was about 43 Hz (see Figure 2). Even at x/D = 0.2, Figures 7a and 7d already showed the difference between their Type A vortices. With the evolution, in Figures 7e and 7f, the Type A vortices propagated and amplified slowly, whereas in Figures 7b and 7c, the Type A vortices propagated and amplified much faster. A_f was the same (~7%) for the two cases. Figure 7 indicates that the Type A vortices develops much fast under 6 Hz than under 16 Hz (also see Figure 10 below for the corresponding spanwise vortices).

Forcing amplitude A_f influence

Figure 8 shows the influence of A_f under a constant f_f = 5.6 Hz for a mixing layer of U_1 = 10 cm/s and U_2 = 5 cm/s. The white lines in Figure 8 indicate the initial visual spreading angle of the mixing layer. The measured f_{01} was about 7 Hz, and the forcing was in the mode I. As we know, the mixing layer biases to the low-speed side downstream of the trailing edge in the unbounded case. This was also true in Figures 8a and 8b. In Figure 8a there was no forcing and in Figure 8b the flow was forced with A_f being about 1.5%. The vortices were induced by the Kelvin–Helmholtz instability with an initial spreading angle $-\alpha_i$ being about 8°. In Figure 8b the flow displayed the three regions of nonlinear spreading observed by Fiedler et al.[33] and Oster and Wygnanski.[25] In region I, corresponding to $0 < x/\theta_0 < 67$ or $0 < x/D < 0.5$, the initial $-\alpha_i$ was about 16°, and doubled the unforced one. In region II, $67 < x/\theta_0 < 406$, or $0.5 < x/D < 3$, the spreading slowed or stopped, that is, $-\alpha_i$ became zero. In region III, $x/\theta_0 > 406$ or $x/D > 3$, the spreading assumed the unforced $-\alpha_I$, which indicated that without forcing or with forcing of relatively low A_f, the confined mixing layer still exhibited a spreading rate similar to that of the two-dimensional mixing layer. In Figure 8c, where A_f was about 5%, $-\alpha_i$ increased to 20°, and the vortices following the trailing edge were almost no longer the pure Kelvin–Helmholtz vortices, even though the mixing layer still biased to the low-speed side. This was at a critical point, where the primary vortex had no more the single sign, but

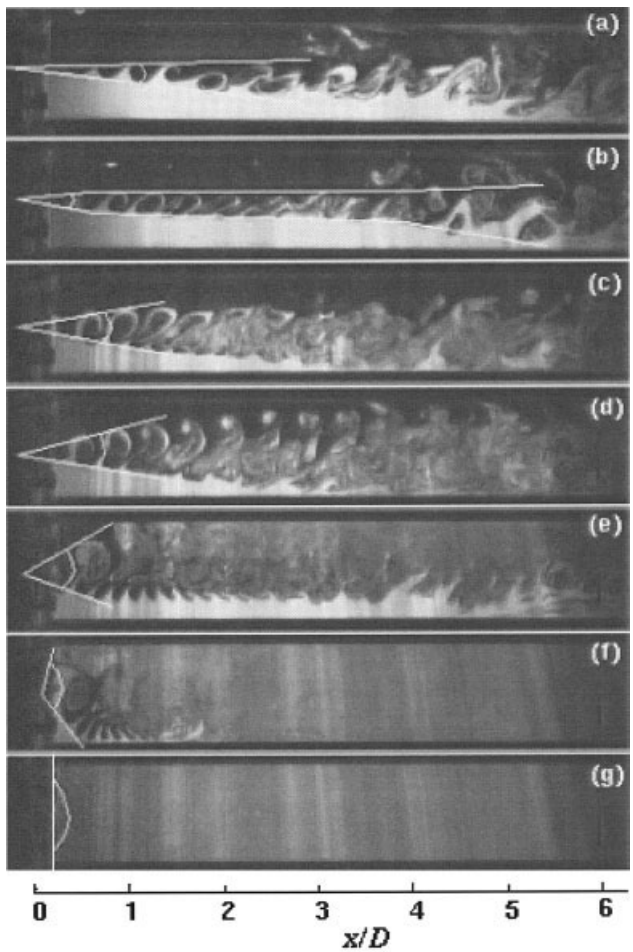

Figure 8. Influence of A_f under f_f = 5.6 Hz for the mixing layer of U_1 = 10 cm/s and U_2 = 5 cm/s.

(a) A_f = 0 (unforced case); (b) 1.5%; (c) 5%; (d) 8%; (e) 18%; (f) 32%; (g) 52%.

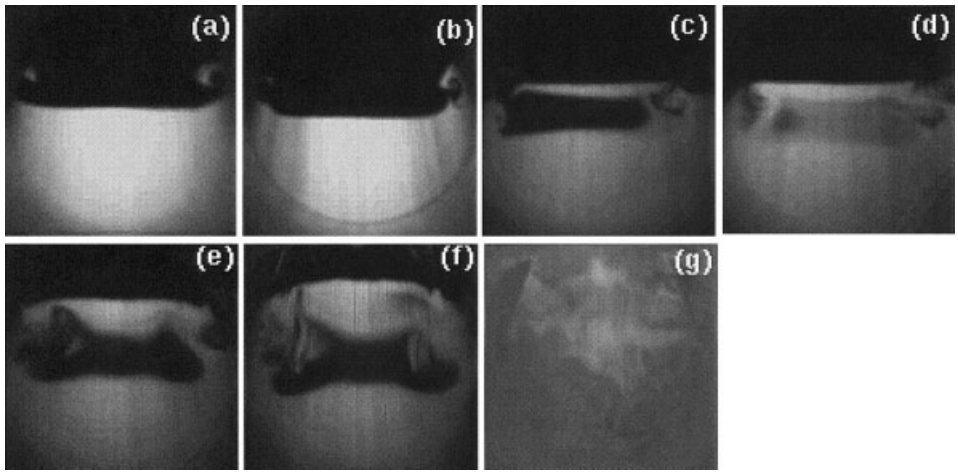

Figure 9. Response of the streamwise vortices to A_f in the mixing layer of $U_1 = 10$ cm/s, $U_2 = 5$ cm/s, at $f_f = 5.6$ Hz and $x/D = 0.2$.

(a) $A_f = 0$ (unforced case); (b) 1.5%; (c) 5%; (d) 8%; (e) 18%; (f) 32%; (g) 52%.

turned out to be an asymmetric counterrotating vortex pair. The right-side vortex was very clearly visible and the left-side one was still not. At about $x/D = 1.2$, the mixing layer did not spread in the high-speed side, but only in the low-speed side until the wall at $x/D = 3$.

In Figure 8d where A_f was around 8%, the asymmetric counterrotating vortex pair became apparent, and the visual mixing layer no longer biased to the low-speed side. Compared with Figure 8c, the mixing layer expanded to the high-speed side, keeping the low-speed side almost unchanged and the $-\alpha_i$ increased to 23°. The three regions during the development in Figure 8b disappeared. In this case, the visualized mixing layer was almost symmetrical to the trailing edge like a wake, but was clearly different from that of the Karman vortex street. As we know, for strong forcing, the instantaneous view of the mixing layer usually shows a nonlinear spreading in the near field as in Figure 8b. However, Figure 8d showed an approximately linear symmetric spreading even though this was an instantaneous view under strong forcing. From this point on, with the further increase of A_f, the primary spanwise vortices in the mixing layer were no longer the pure Kelvin–Helmholtz vortices, but asymmetric counterrotating vortex pairs.

When A_f was increased to 18%, the visual mixing layer surprisingly began to bias to the high-speed side, as displayed in Figure 8e, and the counterrotating vortex pair became larger and clearer. Compared with Figure 8d, the mixing layer in Figure 8e spread to the high-speed side rapidly until the wall at the initial stage with $-\alpha_i$ being about 50°. The fluid in the high-speed side was vigorously stirred, but the mixing layer had almost no spreading in the low-speed side and the fluid there remained unstirred until $x/D \approx 4.2$. The mixing was greatly increased in the high-speed side, but decreased in the low-speed side compared with Figure 8d.

When A_f was around 32%, Figure 8f shows that only the first counterrotating vortex pair beyond the trailing edge was distinguished and the $-\alpha_i$ was about 128°. No large structure could be seen after $x/D \approx 1.5$ as a result of the dramatic mixing. The mixing layer still spread to the low-speed side. It is worth mentioning that the large vortex immediately downstream of the trailing edge here was not attributed to "collective interaction " because the forcing frequency is in mode I, where merging of many vortices could not be possible. The large vortex was actually an asymmetric counterrotating vortex pair here.

Finally, when A_f was increased to about 52% the disturbance was so strong that the flow had already become turbulence immediately downstream of the trailing edge, as shown in Figure 8g (if it were not turbulence, there should have been a clearly defined separation line between the two streams or an obvious large structure near the trailing edge). This was also confirmed by the measurement of the scalar power spectrum.[15] The corresponding $-\alpha_i$ seemed to achieve its climactic mixing state, that is, about quasi-180 ° for this situation. Here the quasi-180 ° spreading angle means that the momentum transfer between the initial two streams is so strong that there is no longer a free stream or unmixed scalar in large scale immediately downstream of the trailing edge; The scalar distribution in the whole transverse direction immediately downstream of the trailing edge is almost homogeneous because of the rapid mixing. This is the most exciting result for mixing enhancement. No large structure could be seen immediately downstream of the trailing edge because of the dramatic turbulent mixing. A quantitative measurement of high spatial resolution of about $(4\ \mu m)^3$ with laser-induced fluorescence[15] also showed that the concentration distribution along transverse direction was approximately homogeneous at a given downstream position near the trailing edge, with small-scale structures filling the whole flow field in the cross section. This actually corresponds to the culminant state that turbulence control can achieve to enhance mixing, at least on the large scale.

These phenomena of unusual bias and dramatic mixing under strong forcing of near 6 Hz would be related to the streamwise Type A vortices as displayed in Figure 9, which is the cross-view of Figure 8 at $x/D = 0.2$. The unforced situation is shown in Figure 9a. Figure 9b exhibited the case with forcing A_f of about 1.5%. No distinguishing difference for Type A vortices could be observed between Figures 9a and 9b except that the interface between the high and low speed was more distorted near the Type A vortices in Figure 9b. However, in

Figure 9c, where A_f was about 5%, the Type A vortices apparently amplified, and the size difference between the vortices of the counterrotating vortex pairs from the high- and low-speed sides became smaller. This situation corresponded to the case where the primary counterrotating vortex pair in the side view of Figure 8c began to emerge. When A_f was increased to 8%, as shown in Figure 9d, the Type A vortices propagated not to the axis of the pipe as in the case of wake of $\lambda = 0$, but to the high-speed side at a small angle. Under the same condition, the mixing layer in Figure 8d began not to bias to the low-speed side. In Figure 9e, A_f was about 18%, the angle was increased and the mixing layer was biased to the high-speed side. The size of the Type A vortices in Figure 9e was larger than that in Figure 9d. With further increase of A_f to around 32%, the Type A vortices were further increased, as shown in Figure 9f, and the sizes of the Type A vortices of the low- and high-speed sides were almost the same. Until A_f was around 52%, the disturbance was so strong, that the Type A vortices were rapidly amplified and broken down. The flow was turbulence and no distinguishing large structures of the Type A vortices could be observed. The result indicated that the primary and secondary counterrotating vortices could be correlated to each other.

Figure 9 indicates that the Type A vortices and the spanwise structures positively gave impulse back to strengthen each other. It seems that the Type A vortices were very sensitive to the strong forcing with $f_f = 6$ Hz without apparent saturation before the state of Figure 9g was achieved. The Type A vortices could be the reason for the dramatic spreading of the mixing layer. Although the bias of the Type A vortices and the spanwise structure are related to each other, as shown in Figures 8 and 9, it is not clear which is the original cause.

The effect of A_f on spanwise structures depended strongly on values of f_f similar to those of the streamwise vortices in Figure 7 and it was only when f_f was near 6 Hz for the present setup that the A_f became very effective, especially for strong forcing. This is shown in Figure 10, which displays the effects of A_f for $f_f = 6$ Hz and 16 Hz, $U_1 = 30$ cm/s, and $U_2 = 20$ cm/s, respectively. The f_{01} for the Kelvin–Helmholtz instability was estimated to be 43 Hz; thus the forcing at 16 Hz corresponded to mode II of the Kelvin–Helmholtz instability.

Figure 10a is the unforced mixing layer. From Figures 10b to 10f, the flow was forced with $f_f = 6$ Hz. In Figure 10b, where A_f is around 1.5%, the collective interaction was clearly visible because f_f was much lower than f_{01}. A_f was about 7% in Figure 10c. It was the critical point where the collective interaction was almost not visible. The visual $d\delta_v/dx$ increased very fast downstream in the initial stage as A_f rose. The corresponding fast developing of the Type A vortices in Figure 10c is shown in Figures 7a, 7b, and 7c. In Figure 10d, A_f was so high ($\sim$16%) that the asymmetric counterrotation vortex pair mentioned earlier formed immediately downstream of the trailing edge and no collective interaction could be seen. The saturation of A_f had still not emerged. In Figure 10e, where A_f was about 40%, $d\delta_v/dx$ was further increased. In this case, the first counterrotating vortex pair was already broken down because of the strong disturbance, although the leg of the first counterrotating vortex pair was still distinguished immediately downstream of the trailing edge. When A_f was increased to about 50%, the mixing layer spread immediately to the wall of both sides, as shown in Figure 10f. Thus $-\alpha_i$ became approximately quasi-

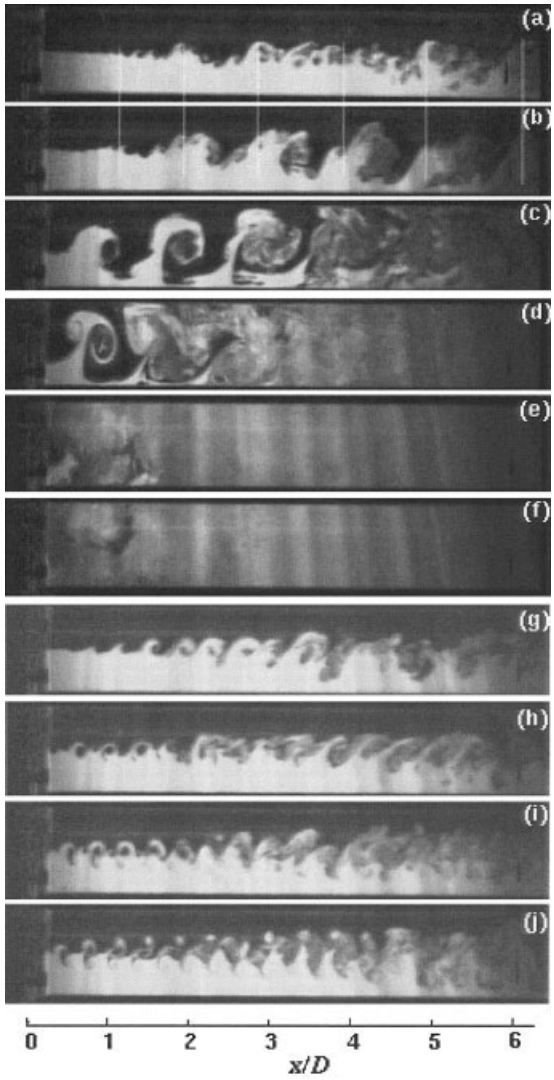

Figure 10. Comparison of the different evolution of the mixing layer at $f_f = 6$ and 16 Hz, respectively, with $U_1 = 30$ cm/s and $U_2 = 20$ cm/s.

$f_f = 6$ Hz: (a) $A_f = 0$ (unforced case); (b) 1.5%; (c) 7.0%; (d) 16%; (e) 40%; (f) 50%. $f_f = 16$ Hz (mode II of conventional Kelvin–Helmholtz instability): (g) $A_f = 7.0\%$; (h) 16%; (i) 40%; (j) 50%.

180°, implying that the flow was not saturated even at $A_f =$ 40%.

Note that, although the flow was an unforced mixing layer and its f_{01} was 43 Hz, Figure 10a demonstrates also the quasi–6 Hz of the primary structure (indicated by the vertical lines) compared with Figure 10b, where the quasi-periodic large structures corresponded to the forced structures of 6 Hz as a consequence of the strong forcing. Because the two pictures had approximately the same phase angle of the structures, the quasi–6 Hz structures in Figure 10a could be distinguished by the vertical lines.

However, the influence of A_f on the development of the mixing layer showed quite different behavior, when f_f was 16 Hz, as displayed in Figures 10g–10j. The forcing A_f from Figures 10g–10j were around 7, 16, 40, and 50%, respectively. In Figure 10g, where A_f was around 7%, the forced flow was

similar to that of a forced conventional two-dimensional mixing layer. Compared with Figure 10a, the forced $d\delta_v/dx$ in the near field in Figure 10g was increased. However, compared with Figure 10c, $d\delta_v/dx$ in Figure 10g was apparently smaller, even though both had the same value of A_f. Figures 7d, 7e, and 7f showed the corresponding relatively slow developing of Type A vortices. This could confirm that the amplification of spanwise structures was closely related to their corresponding Type A vortices. As A_f was increased to 16%, there was only a small change of $d\delta_v/dx$ within $x/D = 2$ because of the very high A_f, which made the initial wake of the mixing layer (there is an initial wake in mixing layer[26]) distinguished in Figure 10h. Because the amplification of the initial wake was very small, it disappeared further downstream because of the velocity difference between the two streams in the mixing layer. Therefore in this case the initial wake has no strong influence on the mixing layer. With further increase of A_f to 40 and 50%, respectively, in Figures 10i and 10j, no further increase in $d\delta_v/dx$ could be obtained because of the well-known saturation. In a comparison of Figures 10g, 10h, and 10i, we found no distinguishing difference along their values of $d\delta_v/dx$, considering the development of the mixing layer further downstream. The visualization from Figures 10g–10j indicated that the mixing layer was nearly saturated to A_f in the range of 7–16%, similar to that of the conventional two-dimensional mixing layer (see, for example, Fiedler and Mensing[27]) despite the confinement. In general, all values of $d\delta_v/dx$ with $f_f = 16$ Hz were much smaller than those with $f_f = 6$ Hz.

Note that, although there is also the primary counterrotating vortex pair in Figure 10h, whose origin is attributed to the strong forcing, here we are interested in the dynamics of the counterrotating vortex pairs, which saturates in Figure 10h with the further increase of A_f for $f_f = 16$ Hz. However, the primary counterrotating vortex pair does not saturate in Figure 10d (also in Figure 8), yet for $f_f = 6$ Hz at the same A_f.

Velocity ratio λ

As we have already seen from Figures 8c and 8d, when A_f was sufficiently high, there would be asymmetric counterrotating vortex pairs for the primary structures and they were not the pure Kelvin–Helmholtz vortices. Measurement disclosed that the A_f needed to cause the counterrotating vortex pair, increased with λ, as shown in Figure 11, where $\bar{U}$ was 7.5 cm/s. This critical A_f was denoted by A_{fc2}. It was also found that λ had no apparent influence on f_{02}; that is, f_{02} was almost independent of λ. With the increase of the velocity ratio, the initial disturbance amplifies faster and the bias of the mixing layer to the low-speed side could become stronger. Thus it would need more energy to change the trend of the mixing layer development. This would be one reason why A_{fc2}, required to generate the asymmetric counterrotating pair of the spanwise structures, increases with the velocity ratio.

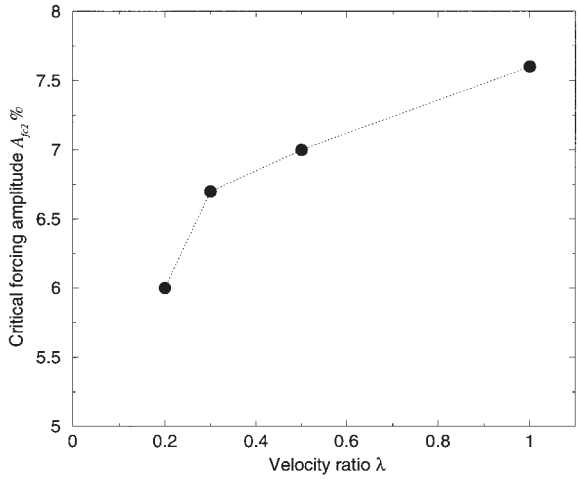

Figure 11. Critical forcing amplitude A_{fc2} required to cause asymmetric counterrotating vortex pair of the primary vortices increases with λ for $Re_{\theta_0} = 22$.

Discussion

Some comments on the experimental observations

From the measurement of the most-probable frequency f_{01}, the observed response of the mixing layer to the forcing frequency f_f (except the narrow band near 6 Hz) and forcing amplitude A_f, we find that the confined mixing layer in a pipe also obeys the Kelvin–Helmholtz instability in the initial stage, and its development is qualitatively similar to that observed in a conventional two-dimensional mixing layer in the near field, although this is a highly three-dimensional mixing layer. However, in the confined configuration, the power spectrum has an extra peak at the narrow-frequency band near 6 Hz, which is independent of the mean flow velocity. The observation of more than one peak in the spectrum is no surprise, even if they are incommensurable. However, the point of interest is that when the flow is forcing at the narrow-frequency band some new phenomena have been observed, which have not been reported either in the conventional two-dimensional mixing layers or in confined three-dimensional mixing layers.

Fiedler et al.[33] observed the same excitation behavior for all frequencies used. Fiedler and Mensing[27]also found that the flow was not frequency selective. The response of the mixing layer to forcing is frequency dependent only inasmuch as the downstream position of saturation is inversely proportional to the forcing frequency. Ho and Huang[26] found that the forcing frequency had the most pronounced effect on the mixing layer. In the initial region, the instability frequency of the forced mixing layer was not necessarily the same as the forcing frequency. The initial response frequency is seen to correspond to that particular harmonic of the forcing frequency that is nearest to, but smaller than, the natural frequency. Simultaneous merging of as many as two, three, or four vortices can be promoted through subharmonic forcing of the most-amplified frequency. Figures 4 and 10 display not only a forcing frequency effect similar to that in Ho and Huang,[26] but also a different and specific forcing frequency effect around the narrow-frequency band.

There are few publications for the influence of large forcing amplitude on mixing layer evolution. Oster and Wygnanski[25] showed a saturation trend of the forcing amplitude influence and also suggested that at larger forcing amplitude the mixing layer resonated with the imposed oscillation in region II. Fiedler and Mensing[27] studied the influence of forcing amplitude and found that in a plane mixing layer, the effect of the forcing

amplitude reached saturation when it was as high as 6.5%. With respect to the mean, the forced flow always experienced stronger spread than the neutral one. It was approximately twice the neutral value and independent of the forcing amplitude. However, Figure 8 indicates that there was no such saturation and $d\delta_{v'}/dx$ depended strongly on A_f for the forcing around 6 Hz. $d\delta_{v'}/dx$ under strong forcing could be far larger than twice that of the neutral one. If the forcing is higher than this narrow-frequency band (such as at 9 Hz in Figure 4f), the receptivity will be negligible or there may be no receptivity at all, even though A_f is very high. Thus, the results here indicate that A_f also has a strong influence on the confined mixing layer, but mostly near a constant frequency, that is, 6 Hz for the present setup.

Fiedler et al.[33] reported that forcing causes the strongest spreading on the low-speed side of a mixing layer. To the author's knowledge, no publication has shown that the mixing layer could keep symmetrically to the trailing edge and even bias to the high-speed side as shown in Figure 8e.

Ho and Nosseir[38] observed a phenomenon called "collective interaction," under which the shear layer displayed an extremely large spreading rate. To achieve the collective interaction, the required A_f should be very high and f_f much lower than f_{01}. Ho and Huang[26] further pointed out that if A_f was extremely high and close to the saturation level, the mixing layer could directly form a large vortex. Although Figures 8e and 8f display a large vortex immediately downstream of the trailing edge, the collective interaction should not be the reason for such a large spreading of the shear layer. This is explained by the fact that f_f (=5.6 Hz) here is in mode I and its value is only 0.78 times that of f_{01}, that is, it is not a very low frequency. Although f_f (=6 Hz) is much smaller than f_{01} in Figure 10b and the collective interaction occurs therein, the A_f is still not saturated in Figure 10d. Thus the collective interaction observed in Figure 10 is only a coincidence with the fast spreading rate for forcing at the narrow-frequency band. The response of the mixing layers to A_f in Figure 8 with f_f = 5.6 Hz and Figure 10 with f_f = 6 Hz should have the same mechanism, although their λ and Re_{θ_0} are different.

According to the published common and limited range of the spreading rate in mixing layers, Browand and Ho[34] proposed a quasi-universal spreading rate for mixing layers, which also includes forced situations. Dimotakis[39] remarked that there was a rather large spread of values in the spreading rate of the mixing layer, and that it was even not clear whether the inequality bounds represented the actual limiting values. Normally, in a two-dimensional mixing layer, the spreading angle at the beginning is no larger than 30° when forcing is applied. However, in Figure 8 the spreading angles not only exceed 30°, but also reach to quasi-180° (the limitation for mixing enhancement on a large scale).

All the above discussions could imply that the unusual behaviors with forcing near 6 Hz could be influenced not only by the Kelvin–Helmholtz instability, but also by some unknown effect, whose mechanism is still not elucidated. The large vortex near the trailing edge of the mixing layer can be explained only by the existence of large transverse velocity components v' because its timescale is small from the perspective of kinematics, although visualization alone with high Schmidt number could be misleading in the far field.[40] If v' is high with forcing, it could indicate that more disturbance from the forcing is absorbed and converted into v' at the trailing edge by the system. Because receptivity describes how environmental disturbances are converted into unstable waves in shear flows—that is, an issue of instability—we would assume that for a given A_f, the higher v', the larger the receptivity of the flow. Because the confined mixing layer has very large vortices at the trailing edge only when the forcing is at the narrow-frequency band, we would assume that the flow has higher receptivity at the narrow band than at other frequencies. Thus, the response of the confined configuration to the forcing near the narrow-frequency band could be related to some unknown receptivity mechanism.

It seems at first that the narrow band of f_{02} is similar to the frequency of an organ pipe (quasi-excitation) observed by Fiedler and Thies.[41] However, no unusual phenomena mentioned earlier were observed in that work. It is not clear whether the nearly constant f_{02} is the resonance frequency of the water channel. If it is the resonance frequency, there should always be vibration of the channel under strong forcing of the narrow-frequency band irrespective of whether the fluid is at rest or in motion. An experiment was conducted to test this premise. The actuator was driven at 6 Hz with the fluid at rest, and no strong vibration of the channel could be observed compared to the case with flow. This could indicate that 6 Hz might not be the system resonance frequency of the channel. Although the sidewall has a strong influence in the confined configuration, it is also distinguishable from the Tollmien–Schlichting wave (that is often the main reason for wall-boundary flow receptivity and could also be established on the splitterplate and sidewall) because frequency corresponding to the Tollmien–Schlichting wave is also related to the mean flow velocity. The feedback mechanism in Ho and Huerre[23] could not be relevant because no primary vortex merging can be observed under strong forcing at 6 Hz, as shown in Figure 8. The quasi-periodic flow near the narrow-frequency band might be related to the three-dimensional property of confined mixing layer, the experimental setup, and natural frequency of the pipe.

Finally, it is necessary to mention that, even if the mechanism of the confined mixing layer development under forcing near the narrow-frequency band is not clear, one thing is already obvious: the extraordinarily rapid mixing is very appealing for mixing enhancement and would provide broader opportunities for technologies, where fast mixing is required. For instance, the corresponding mixing process also has most of the advantages of those micromixers, which are now poised to generate big waves in the biotechnology, chemical, and pharmaceutical industries.

Streamwise vortices

The streamwise vortices that superimposed onto the spanwise eddies in the mixing layer were first observed by Miksad.[42] For the origin of the streamwise vortices, Breidenthal[43] noted a wiggle disturbance in the outer edge of the primary vortices, from which the longitudinal streaks originated as a result of "the global strain field of the flow." Bernal and Roshko[44] regarded the appearance of streamwise vortices as uninfluenced by upstream conditions, indicating that far enough downstream of the splitterplate, the streamwise vortices (or riblike structure[45]) might result from an instability of the

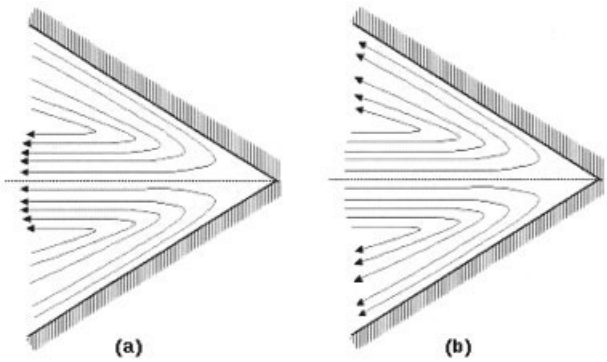

Figure 12. Model of the secondary flow along the streamwise corner.

(a) Laminar flow; (b) turbulent flow.

primary vortices. Jimenez[46] suggested that the streamwise vortices tended to lock onto small geometric details in the experimental apparatus. Lasheras et al.[47] found experimentally that the origin of streamwise vortices could be changed by control of the spanwise vorticity distribution in the splitterplate (spanwise upstream) and could be moved considerably upstream by the mounting of small vortex-generating elements on the splitterplate. Having a spanwise-periodic forcing, Nygaard and Glezer[28] observed the streamwise vortices downstream of the trailing edge, but upstream of the first rollup of the spanwise vortices. However, few studies have addressed the sidewall effect on the streamwise vortices except the works from Roberts[48] and Lasheras and Maxworthy.[49] Furthermore, the influence of the corner flows between the splitterplate and nozzle sidewall has, to the author's knowledge, never been addressed in detail. The present work finds that the corner flow could have a significant effect on the streamwise vortices in the confined configuration.

The origin of the Type A vortices observed in the present study seems to be different from either that of conventional streamwise vortices, or those observed by Roberts[48] and Lasheras and Maxworthy.[49] It could be helpful to consider a tentative and simplified model for the origin of Type A vortices to consider the corner flow effect. In the confined configuration, the streamwise corner flow along the junction of the trailing edge and the nozzle sidewall and its interaction with the primary vorticity immediately downstream of the trailing edge determine the topology of Type A vortices. The streamwise corner flow along the junction of two plates is itself subject to instability because of the inflectional nature of the streamwise velocity profile.[50,51] The corner flow is characterized by its secondary flow, which depends on whether the boundary flow is laminar or turbulent. For the laminar corner flow, the secondary flow moves outward from the corner along the plane of symmetry and inward toward the corner close to the walls,[52] as shown in Figure 12a. The secondary flow in a turbulent corner flow is opposite to that of the laminar corner flow,[53] as shown in Figure 12b.

The vorticity of the corner flow leaving the trailing edge will interact with the vorticity of the primary flow in a complex manner. The generated structures depend on the trailing edge geometry, flow state (that is, laminar or turbulent flow in the corner), the type of flow (wake with $\lambda = 0$ or mixing layer), with or without forcing, and so on. The sharp trailing edge was used here. Without forcing, the corner flow could be laminar in the present experimental range of Reynolds number because the favorable pressure gradient can stabilize the corner flow.[54] If the primary flow is wake ($\lambda = 0$), the boundary vorticity on both sides of the trailing edge is the same value with different sign. There will be two streamwise counterrotating vortex pairs on each side of the pipe wall as shown in Figure 13a. Figure 13b shows an example of a wake flow of $\bar{U} = 7.5$ cm/s without forcing from visualization. However, if the primary flow is a mixing layer, there will be only one streamwise counterrotating vortex pair (two signs) at each side of the wall, as shown in Figures 13c and 5a, resulting mainly from the high-speed side. This could be because the boundary vorticity of the high-speed side of the trailing edge is higher than that of the low-speed side and the low vorticity will be subsumed into the high one, as suggested by Roberts[48] and Lasheras and Maxworthy.[49] However, the model proposed here is different from that of Roberts,[48] where it was assumed that the vortex was only one sign for the mixing layer and one counterrotating vortex for the wake. It is also different from the perspective view of Lasheras and Maxworthy,[49] where it seemed that the vortex was also assumed to be one sign in the mixing layer based on the interaction of the side wall and the plane shear layer. Therefore, it seems that the fundamental issue of the sidewall effect on the streamwise vortices in the mixing layer needs further study.

With sufficiently high forcing amplitude, the impulse in the transverse direction at the trailing edge becomes high as a result of the possible large receptivity at the trailing edge, which converts the forcing energy into the transverse velocity component. For the wake with $\lambda = 0$, this impulse will in turn, because of the confinement, positively give the impulse (and thus enhance) only those vortices that have the same sign with the impulse, although there is originally a counterrotating vorticity pair along each corner. Therefore, only one counterrotating vortex pair of Type A vortices is yielded, as shown in Figure 14a at each side of the pipe wall (experimental evidence is given in Wang[15]). This is also identical to the experimental evidences from Roberts[48] and Mackinnon and Koochesfahani.[55] For the mixing layer, the strong forcing enhances not only the impulse, but also its initial wake, which is so strong that the Type A vortices in the mixing layer become similar to that in a wake with $\lambda = 0$, as shown in Figures 14b and 6a. The Type A vortices shown in Figure 14 could be applied to both

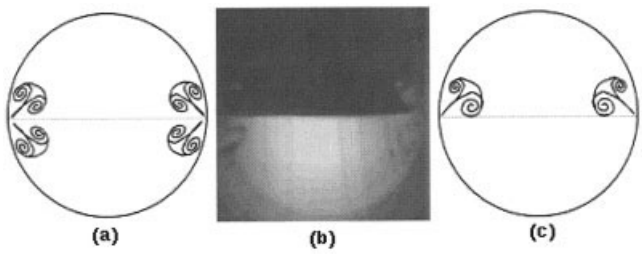

Figure 13. Model of the streamwise Type A vortices of the unforced flows downstream of the trailing edge.

(a) Unforced wake; (b) visualization result of a wake of $\bar{U} = 7.5$ cm/s without forcing at $x/D = 0.2$; (c) unforced mixing layer.

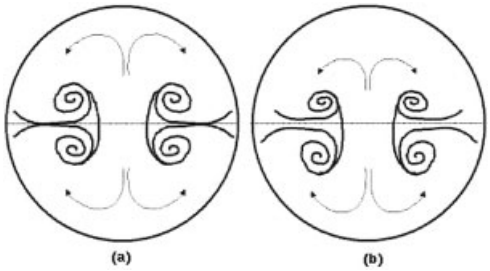

Figure 14. Model of the streamwise Type A vortices of the forced flows downstream of the trailing edge.

(a) Forced wake; (b) forced mixing layer.

laminar and turbulent corner flow for sufficiently high forcing amplitude. This simplified model could explain the observed origin and evolution of Type A vortices and indicate the importance of the initial wake, the corner flow, and sidewall effect.

The extremely fast spreading of the mixing layers could be related to the Type A vortices. This can also be seen by referring to Figures 7 and 10, which show that $d\delta_v/dx$ is much higher at 6 Hz than at 16 Hz. Figures 8 and 9 show that the primary and streamwise Type A vortices have approximately the same size in the transverse direction immediately downstream of the trailing edge. Figures 7 and 10 show that when spanwise vortices develop fast, so do the Type A vortices, and both develop fast when forcing frequency is at 6 Hz with sufficiently high forcing amplitude. These indicate that the fast spreading of the confined mixing layer is related to the Type A vortices. Figure 9 could also imply that the forcing introduces an impulse in transverse direction that, in turn, can enhance the development of the Type A vortices because of the confinement. The development of the Type A vortices favors the amplification of the spanwise structure and thus these two kinds of vortices impulse each other positively. Thus the formation of the three-dimensional mixing layer is accelerated.

Confined configuration

The investigations of the sidewall effect on the dynamics of the mixing layer in the confined configuration are limited, except a few works from Wood and Bradshaw,[56] Veynante et al.,[57] and Koochesfahani and Mackinnon.[55] However, the novel phenomena observed in the present study have not been reported in these works. Although Wood and Bradshaw[56] were concerned about the sidewall effect, no active forcing was applied to investigate the corresponding dynamic behavior. Usually such flows are not considered of general interest for fundamental research because additional complications of the sidewall influence are introduced, which may obscure the study of turbulence mechanisms. In all realistic cases, however, the sidewall influence is always present, albeit often only to a negligible extent, and it may not be unwelcome under all circumstances. For instance, the confined mixing layer can provide extremely fast mixing.[16] In relatively low Reynolds number (about 400 based on pipe diameter and mean velocity) under strong forcing of around 6 Hz, the flow exhibits the $-5/3$ Oboukhov–Corrsin spectrum in the near field. Therefore, we could study local homogeneous isotropic turbulence in relatively low Reynolds number flow, and thus the spatial resolution for experimental measurement of scalar in turbulent flow could be substantially improved.[15]

Summary and Conclusion

It seems that the confined mixing layer in a pipe is an interesting flow. On the one hand, even if the confined configuration is a three-dimensional mixing layer, it obeys the Kelvin–Helmholtz instability and behaviors qualitatively similar to the traditional two-dimensional mixing layer in the near field when the flow is not forced or is forced based on the conventional forcing mechanism (or receptivity). On the other hand, we also find that in the confined configuration, there is an extra peak in the scalar power spectrum in a very narrow frequency band around a nearly constant frequency, which is not commensurate with the most-probable frequency and is independent of the mean flow velocity. Under strong forcing within this narrow-frequency band, several new phenomena are observed, which are different from those observed in two-dimensional mixing layers: the forcing could cause the mixing layer not to bias to the low-speed side, but be symmetric to the trailing edge or even bias to the high-speed side; the spreading rate is extremely high and can even be as high as quasi-180° immediately downstream of the trailing edge of the mixing layer without the limitation of the well-known saturation, resulting in a rapid turbulent mixing, which can at best be achieved through turbulence control for mixing enhancement. These novel observations can be obtained only when the forcing is within the narrow frequency band.

The streamwise vortices—that is, the Type A vortices—play an important role for the mixing layers evolution in the confined configuration, especially under strong forcing because they are related to the unusual phenomena observed for the spanwise large structures. The Type A vortices, which are counterrotating vortex pairs, originate from the interaction of the vorticity stemming from the corner flow between the splitterplate and the pipe wall, and the vorticity of the large spanwise structures of the mixing layer immediately downstream of the trailing edge. They amplify very fast in the initial stage, resulting in the dramatic spreading of the primary structures, also only under the forcing of the narrow frequency band. However, the mechanism of the new observation and the extent of sidewall effect are still not clear. The quantitative velocity field has not been measured. Further investigations are needed to study the mechanism and scaling law behind the forcing within the narrow-frequency band.

Acknowledgments

The author first thanks his advisor, the deceased Prof. H. E. Fiedler, for his advice and support of the work, and expresses appreciation to Professor H. Zhou from Tianjing University/China, who initially inspired and advised him to study the instability theoretically when he was in Berlin. Discussion with him was very helpful. Professor J. S. Luo from Tianjing University/China gave the author substantial help both in doing the experiment and discussion of the problems, when he was in Berlin. The author also thanks Professor M. Kawaji from University Toronto for providing equipment to collect images when he was in Toronto. Discussions with Professors H. Eckelmann, A. Michalke, I. Wygnanski, P. Huerre, M. D. Zhou, J. T. C. Liu, P. Bradshaw, and J. Jemenez are also very much appreciated.

Literature Cited

1. Brodkey RS. *Turbulence in Mixing Operations: Theory and Application to Mixing and Reaction*. New York, NY: Academic Press; 1975.
2. Hill JC. Homogeneous turbulent mixing with chemical reaction. *Annu Rev Fluid Mech.* 1976;8:135-161.
3. Baldyga J, Bourne JR. *Turbulent Mixing and Chemical Reactions*. New York, NY: Wiley; 1999.
4. Ottino JM. Mixing, chaotic advection, and turbulence. *Annu Rev Fluid Mech.* 1990;22:207-253.
5. Coats CM. Coherent structures in combustion. *Prog Energy Combust Sci.* 1996;22:427-509.
6. Fiedler HE, Fernholz HH. On management and control of turbulent shear flows. *Prog Aerospace Sci.* 1990;27:305-387.
7. Eaton WA, Munoz V, Hagen SJ, Jas GS, Lapidus LJ, Henry ER, Hofrichter J. Fast kinetics and mechanism in protein folding. *Annu Rev Biophys Biomol Struct.* 2000;29:327-359.
8. Oldshue JY. *Fluid Mixing Technology*. New York, NY: McGraw-Hill; 1983.
9. Harnby N, Edwards MF, Nienow AW. *Mixing in the Process Industries*. Oxford, UK: Butterworth-Heinmann; 1992.
10. Schetz JA. *Injection and Mixing in Turbulent Flow*. Reston, VA: American Institute of Aeronautics and Astronautics; 1980.
11. Forney LJ. Jet injection for optimum pipeline mixing. In: Cheremisinoff NP, ed. *Encyclopedia of Fluid Mechanics*. Houston, TX: Gulf Publishing; 1986:660-690.
12. Ottino JM, Muzzio FJ, Tjahjadi M, Franjione JG, Jana SC, Kusch HA. Chaos, symmetry, and self-similarity: Exploiting order and disorder in mixing processes. *Science.* 1992;257:754-760.
13. Shinbrot T, Alexander A, Moakher M, Muzzio FJ. Chaotic granular mixing. *Chaos.* 1999;9:611-620.
14. Harvey AP, Mackley MR, Stonestreet P. Operation and optimization of an oscillatory flow reactor. *Ind Eng Chem Res.* 2001;40:5371-5377.
15. Wang GR. *Turbulent Mixing, Stability and Secondary Flow in a Confined Configuration*. Band 8. Berlin: Verlag Dr. Köster; 2000.
16. Wang GR. A rapid mixing process in continuous operation under periodic forcing. *Chem Eng Sci.* 2003;58:4953-4963.
17. Brown GL, Roshko A. On density effects and large structure in turbulent mixing layers. *J Fluid Mech.* 1974;64:775-816.
18. Winant CD, Browand FK. Vortex pairing: Mechanism of turbulent mixing layer growth at moderate Reynolds number. *J Fluid Mech.* 1974;63:237-255.
19. Michalke A. On spatially growing disturbance in an inviscid shear layer. *J Fluid Mech.* 1965;23:521-544.
20. Michalke A. Instabilitaet eines kompressible runden Freistrahs unter Berueksichtigung des Einiflussess der Strahgrenzschichtdicke. Z *Flugwiss.* 1971;19:319-328.
21. Bechert DW. Excitation of instability waves in free shear layers. I—Theory. *J Fluid Mech.* 1988;186:47-62.
22. Huerre P, Monkewitz PA. Local and global instabilities in spatially developing flows. *Annu Rev Fluid Mech.* 1990;22:473-537.
23. Ho CM, Huerre P. Perturbed free shear layers. *Annu Rev Fluid Mech.* 1984;16:365-423.
24. Oster D, Wygnanski I, Dziomba B, Fiedler H. The effects of initial conditions on the two-dimensional mixing layer. In: Fiedler H, ed. *Structure and Mechanisms of Turbulence I*. Berlin: Springer-Verlag; 1978.
25. Oster D, Wygnanski I. The forced mixing layer between parallel streams. *J Fluid Mech.* 1982;123:91-130.
26. Ho CM, Huang LS. Subharmonics and vortex merging in mixing layer. *J Fluid Mech.* 1982;119:443-473.
27. Fiedler HE, Mensing P. The plane turbulent shear layer with periodic excitation. *J Fluid Mech.* 1985;150:281-309.
28. Nygaard KJ, Glezer A. Evolution of streamwise vortices and generation of small-scale motion in a plane mixing layer. *J Fluid Mech.* 1991;231:257-301.
29. Wiltse JM, Glezer A. Manipulation of free shear layers using piezoelectric actuators. *J Fluid Mech.* 1994;249:261-285.
30. Cantwell BJ. Organized motion in turbulent flows. *Annu Rev Fluid Mech.* 1981;13:457-515.
31. Dimotakis PE. Two-dimensional shear-layer entrainment. *AIAA J.* 1986;24:1791-1796.
32. Weisbrot I, Wygnanski I. On coherent structures in a highly excited mixing layer. *J Fluid Mech.* 1988;195:137-159.
33. Fiedler HE, Dziomba B, Mensing P, Rösgen, T. Initiation, evolution and global consequences of coherent structures in turbulent shear flows. In: Jimenez J, ed. *The Role of Coherent Structures in Modelling Turbulence and Mixing*. Berlin/New York: Springer-Verlag; 1981.
34. Browand FK, Ho CM. Forced, unbounded shear flows. In: Duong-Van M, ed. *CHAOS'87. International Conference on Physics of Chaos and Systems Far from Equilibrium*. Amsterdam: North-Holland; 1987.
35. Börger G. Optimierung von Windkanaldüsen für den Unterschallbereich. Z *Flugwiss.* 1975;23:45-50.
36. Wang GR, Fiedler HE. On high spatial resolution scalar measurement with LIF. Part 2: The noise characteristic. *Exp Fluids.* 2000;29:265-274.
37. Wang GR, Fiedler HE. The paring burst—A new phenomenon. *Bull Am Phys Soc*. 1996;October:41.
38. Ho CM, Nosseir NS. Dynamics of an impinging jet. Part 1. The feedback phenomenon. *J Fluid Mech.* 1981;105:119-142.
39. Dimotakis PE. Turbulent free shear layer mixing and combustion. In: Murthy B, Curran ET, eds. *High-Speed Flight Propulsion Systems*. Reston, VA: AIAA; 1991.
40. Cimbala JM, Nagib HM, Roshko A. Large structure in the far wakes of two-dimensional bluff bodies. *J Fluid Mech.* 1988;190:265-298.
41. Fiedler HE, Thies HJ. Some observations in a large two-dimensional shear layer. In: Fiedler H, ed. *Structure and Mechanisms of Turbulence I*. Berlin: Springer-Verlag; 1978:108-117.
42. Miksad RW. Experiments on the nonlinear stages of free-shear-layer transition. *J Fluid Mech.* 1972;56:695-719.
43. Breidenthal RE. Structure in turbulent mixing layers and wakes using a chemical reaction. *J Fluid Mech.* 1981;109:1-24.
44. Bernal LP, Roshko A. Streamwise vortex structure in plane mixing layers. *J Fluid Mech.* 1986;170:499-525.
45. Hussain AKMF. Coherent structures and turbulence. *J Fluid Mech.* 1986;173:306-356.
46. Jimenez JA. Spanwise structure in the plane shear layer. *J Fluid Mech.* 1983;132:319-336.
47. Lasheras JC, Cho JS, Maxworthy T. On the origin and evolution of streamwise vortical structures in a plane, free shear layer. *J Fluid Mech.* 1986;172:231-258.
48. Roberts FA. *Effects of Periodic Disturbance on Structure and Mixing in Turbulent Shear Layers and Wakes*. PhD Thesis. Pasadena, CA: California Institute of Technology; 1985.
49. Lasheras JC, Maxworthy T. Structure of the vorticity field in a plane free shear layer. In: Durst F, ed. *Turbulent Shear Flows 5*. New York, NY: Springer-Verlag; 1987:124-168.
50. Dhanak DR. On the instability of flow in a streamwise corner. *Proc R Soc Lond A Phys Sci.* 1993;441:201-209.
51. Balachhandar S, Malik MR. Inviscid instability of streamwise corner flow. *J Fluid Mech.* 1995;282:187-201.
52. Zamir M, Young AD. Experimental investigation of the boundary layer in a streamwise corner. *Aeronaut Q.* 1970;21:313-338.
53. Gessener FB, Jones JB. On some aspects of fully-developed turbulent flow in rectangular channels. *J Fluid Mech.* 1965;23.
54. Zamir M, Young AD. Pressure gradient and leading edge effects on the corner boundary layer. *Aeronaut Q.* 1979;30:471-484.
55. Mackinnon CG, Koochesfahani MM. Flow structure and mixing in a low Reynolds number forced wake inside a confined channel. *Phys Fluids.* 1997;9:3099-3101.
56. Wood DH, Bradshaw PA. Turbulent mixing layer constrained by a solid surface. Part 1. Measurement before reaching the surface. *J Fluid Mech.* 1982;122:57-89.
57. Veynante D, Candel SM, Martin J. Influence of the system response on the coherent structures in a confined shear layer. *Phys Fluids.* 1986; 29:3912-3914.
58. Koochesfahani MM, Mackinnon CG. Influence of forcing on the composition of mixed fluid in a two-stream shear layer. *Phys Fluids A.* 1991;3:1135-1142.

Manuscript received Jan. 1, 2005, and revision received May 23, 2005.